Estuarine, Coastal and Shelf Science 224 (2019) 253–259

Contents lists available at ScienceDirect

Estuarine, Coastal and Shelf Science

journal homepage: www.elsevier.com/locate/ecss

Iron speciation in sediment cores near the Jiulong Methane Reef and its implication

Xia Jing, Fenfen Zhang*, Ying Wu

State Key Laboratory of Estuarine and Coastal Research, East China Normal University, 3663, North Zhongshan Road, Shanghai 200062, PR China

ARTICLE INFO

Keywords:
Iron species
Mössbauer spectrometry
Magnetic susceptibility
Magnetite
Methane seepage
Jiulong methane reef

ABSTRACT

Variability in iron species in marine deposits are excellent geochemical archives for exploring variations in redox conditions during early diagenesis and seepage dynamics over time. Two sediment cores (DS07 and DS08) were collected in the Jiulong Methane Reef, a typical cold seep site that is located in the South China Sea (SCS), and analyzed for iron species using Mössbauer spectrometry and magnetic procedures. Excluding the surface layer (0-10 cm) in DS07, Fe^{2+}/Fe^{3+} ratios indicated that core sediments were under anoxic conditions. The Fe^{2+}/Fe^{3+} and frequency-dependent susceptibility (χ_{fd}) at this site were higher while the total organic matter content (TOC) and magnetic susceptibility (χ) were significantly lower at approximately 170 cm depth. Combined with chromium reducible sulfur (CRS), Fe/Al and sulfur to organic content (S/C) ratios suggested that there was a sulfate-methane transition zone (SMTZ) at approximately 170 cm. Moreover, thermomagnetic analyses indicated that magnetite was the dominant ferrimagnetic mineral at 21–23 cm, 165–185 cm, 213–233 cm and 285–295 cm depths, however, magnetite content was relatively lower between the 165 and 185 cm depth, which suggested that magnetite had been largely transformed to paramagnetic iron minerals during the anaerobic oxidation of methane (AOM) process. The DS08 sediment core was also mostly anoxic , however, no obvious methane seepage activity was observed because the maximum values of Fe^{2+}/Fe^{3+}, Fe/Al, CRS, S/C and the minimum values of TOC and χ did not simultaneously occur at the same depth. The study revealed that the speciation of Fe in sediment cores varied under different redox conditions which was of interest when utilizing iron speciation and magnetic minerals as indicators of historical environmental conditions and seepage activities.

1. Introduction

Cold seeps exist in areas along the ocean floor where methane-rich fluid seepage occurs, which is a widely observed phenomenon in marine sedimentary strata along continental margins (Campbell, 2006; Suess, 2014). The anaerobic oxidation of methane (AOM) and sulfate reduction are key biogeochemical processes in cold seep sites (Boetius et al., 2000; Boetius and Wenzhöfer, 2013). When methane seeps, abnormal AOM-related geochemical activities could result in an increase in sulfide and alkalinity along ambient environments, promoting the transformation of iron-bearing minerals (Borowski et al., 1996; Kasten et al., 1998; Passier et al., 1998; Hu et al., 2014).

Numerous studies have revealed that significant variability in Fe content and the transformation of iron-bearing minerals were directly related to the environmental conditions during early diagenesis (Lyons and Severmann, 2006; Lim et al., 2011). After burial, the oxidation and reduction states of iron could change in accordance to site specific environmental conditions. Hence, relative contents of Fe^{2+} and Fe^{3+} and their ratios could represent the redox conditions in sedimentary columns (Kuno et al., 2002; Zheng et al., 2010). Within methane seepage conditions, hydrogen sulfide (HS^-) is produced by AOM and it reacts with iron-bearing minerals in sediments, resulting in the dissolution of magnetic minerals coupled with the precipitation of minerals containing Fe^{2+}, especially paramagnetic pyrite. Therefore, these processes result in higher Fe^{2+}/Fe^{3+} ratios and lower magnetic susceptibility (χ) values in the sulfate-methane transition zone (SMTZ) (Berner, 1970, 1985; Dewangan et al., 2013). However, under low HS^- conditions, an insufficient supply of HS^- leads to partial pyritization, resulting in the preferential formation of greigite, which has a special magnetic signal (Pyzik and Sommer, 1981; Riedinger et al., 2005; Rowan et al., 2009). Different magnetic minerals could be determined by magnetic analyses, which is important to better understand the geochemical mechanism in AOM-related environments (Novosel et al., 2005; Ellwood et al., 2006; Dewangan et al., 2013).

Mössbauer spectrometry is an invaluable methodology for determining the extent of redox environment through iron species and the

* Corresponding author.
E-mail address: ffzhang@sklec.ecnu.edu.cn (F. Zhang).

https://doi.org/10.1016/j.ecss.2019.04.015
Received 28 February 2018; Received in revised form 1 April 2019; Accepted 11 April 2019
Available online 16 April 2019

relative contents of Fe^{2+} and Fe^{3+} (Coey, 1975; Vandenberghe et al., 1994; Zachara et al., 2004; Zheng et al., 2010; Hu et al., 2015). However, the low Fe and high clay mineral contents limit the identification of specific iron species via Mössbauer spectrometry analysis. Although magnetic analyses of sediment cores have been previously used to trace sediment sources and reconstruct paleo-environmental changes (Bloemendal et al., 1992, 1988), the combination of Mössbauer spectrometry with magnetic analysis has seldomly been used to trace the temporal variation in redox conditions.

The Jiulong Methane Reef in the Dongsha area located on the northern South China Sea (SCS) represents a suitable sedimentary environment for studying the unsteady-state diagenesis processes likely because of seafloor landslides and large-scale cold spring activities (Yan et al., 2006; Li et al., 2013). More recently, methane seepage has been investigated through carbon and sulfur isotopes analyses of pore water, as well as major and trace elements (Ca, Mg, Sr, Fe, Mo and so on) along this sedimentary environment (Hu et al., 2014, 2015; 2017). In this study, we presented geochemical parameters such as Fe^{2+}/Fe^{3+}, Fe/Al, magnetic susceptibility (χ), frequency-dependent susceptibility (χ_{fd}), total organic matter content (TOC), chromium reducible sulfur (CRS), and sulfur to organic content ratio (S/C), in two sediment cores near the Jiulong Methane Reef. By analyzing the iron species and iron-bearing minerals along the vertical sedimentary profiles, we aimed to reveal the historical changes in early diagenesis conditions and explore the application of iron-related proxies for methane seepage activities.

2. Materials and methods

2.1. Study site and sediment sampling

The two sediment cores (DS07 and DS08) were collected by the Guangzhou Marine Geological Survey in September 2013. The sampling stations are showed in Fig. 1. These study sites are located only a few hundred meters from the Jiulong Methane Reef (Fig. 1). The DS07 (22°3.0′N,118°45.3′E) and DS08 (22°2.4′N,118°46.8′E) sediment cores were collected from water depths of 766 and 814 m, respectively. The lengths of DS07 and DS08 sediment cores were 340 and 420 cm, respectively. The sediment core intervals were sliced at 5 or 10 cm depth and immediately stored at −20 °C. All sediment samples were dried at 40 °C and then disaggregated prior to analysis.

2.2. Grain size parameters and TOC measurements

For particle size analyses, hydrochloric acid and hydrogen peroxide were used to remove the carbonate and organic matter. The samples were then measured with a laser size (LS) 100Q laser particle analyzer following ultrasonic dispersion. The TOC was measured by a Vario EL-III element analyzer. Samples were treated with 1 M HCl to remove inorganic carbon prior to analysis. The analytical precision of TOC was < ± 5%.

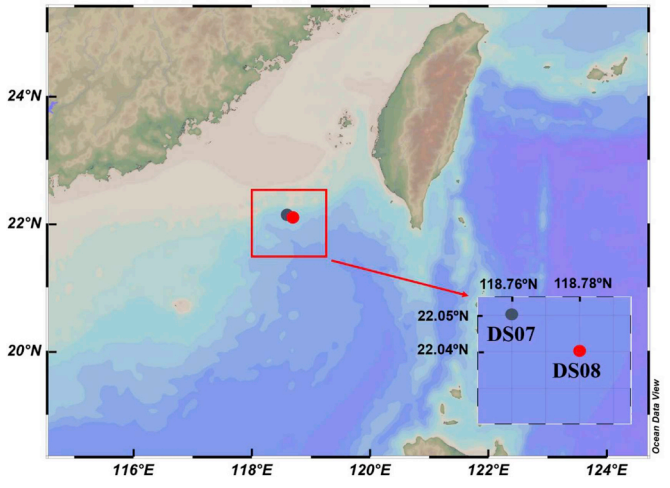

Fig. 1. Map of the study area showing the sediment sampling stations (DS07 and DS08) in the Jiulong Methane Reef of the Dongsha area, South China Sea.

2.3. Mössbauer measurements

Based on previous research, Mössbauer measurements were made for typical depths as shown in Fig. 4 (Hu et al., 2017). Before the ^{57}Fe Mössbauer spectroscopy test was performed, the sediment samples were ground to 100-mesh powder. Then the powder samples were transferred into brass capsules (16 mm in diameter and 1 mm thick; Hu et al., 2015). The Mössbauer spectra were undertaken by a Mössbauer spectrometer using a γ-ray source of 1.11 GBq $^{57}Co/Rh$ at room temperature (293 K) at the Shanghai Institute of Applied Physics, Chinese Academy of Sciences. Isomer shifts were expressed based on the shift of the spectrum center. The obtained Mössbauer spectra were fitted to Lorentzian line shapes using standard line-shape fitting routines, and the intensity and half width of the quadruple doublet peaks were subsequently adjusted (Hu et al., 2015).

2.4. Magnetic properties analyses

To determine the magnetic properties of sediment intervals, low-frequency magnetic susceptibility (χ_{lf}) and high-frequency magnetic susceptibility (χ_{hf}), which are mass-specific, were measured at two different frequencies (0.47 and 4.7 kHz, respectively) using a Bartington MS2B dual-frequency sensor. Frequency-dependent susceptibility (χ_{fd}) was calculated as $\chi_{fd}\% = (\chi_{lf}-\chi_{hf})/\chi_{lf} \times 100$. Measurements of the temperature-dependent magnetization were made using a variable translation field balance (VFTB) by heating to 700 °C, then cooling to an ambient temperature.

3. Results

3.1. Grain size and TOC distribution along the sediment core depths

The grain size compositions of DS07 and DS08 are shown in Fig. 2. The lithology of DS07 was mainly composed of clayey silt and varied greatly with depth, while the lithology of DS08 was mainly composed of clayey silt or silty clay and varied little. The sediment core samples were generally gray in color. In DS07, the mean grain size gradually increased from the surface to ~170 cm depth and then decreased with increasing depth The maximum content was at the ~170 cm depth. However, the mean grain size of DS08 increased until 125 cm and then decreased from 220 to 350 cm. Below 350 cm, the mean grain size sharply increased (Fig. 3). In DS07 and DS08, the profiles of mean grain size showed similar trends with that of sand contents (Figs. 2 and 3). The clay minerals at these two sites were mainly composed of illite, between 58%–67%, followed by chlorite. Smectite and kaolinite were found to be generally very low (Liu et al., 2016).

The accelerating mass spectrometry (AMS) ^{14}C dating results of planktonic foraminifera in DS07 were reported in Hu et al. (2017). The 170 cm and 230 cm were estimated to be ~6.0 cal ka BP and ~7.3 cal ka BP, respectively (Fig. 3). The uncertainties in the ages were within ± 30 yr. Additionally, the foraminifera shell contents increased slowly from the 100 cm and reached maximum values near the 170 cm depth in the DS07 sediment core. Then the foraminifera shell contents decreased gradually from 250 to 320 cm, which corresponded to more sand and silt between 100 and 250 cm depths (Hu et al., 2017). In DS07, the average value of TOC was 0.29%, which initially decreased and then increased to approximately the 170 cm depth from the surface to the bottom (Fig. 3). In DS08, the TOC contents was approximately 0.33% which increased with depth as shown in Fig. 3, coinciding with the trend in clay contents (Fig. 2).

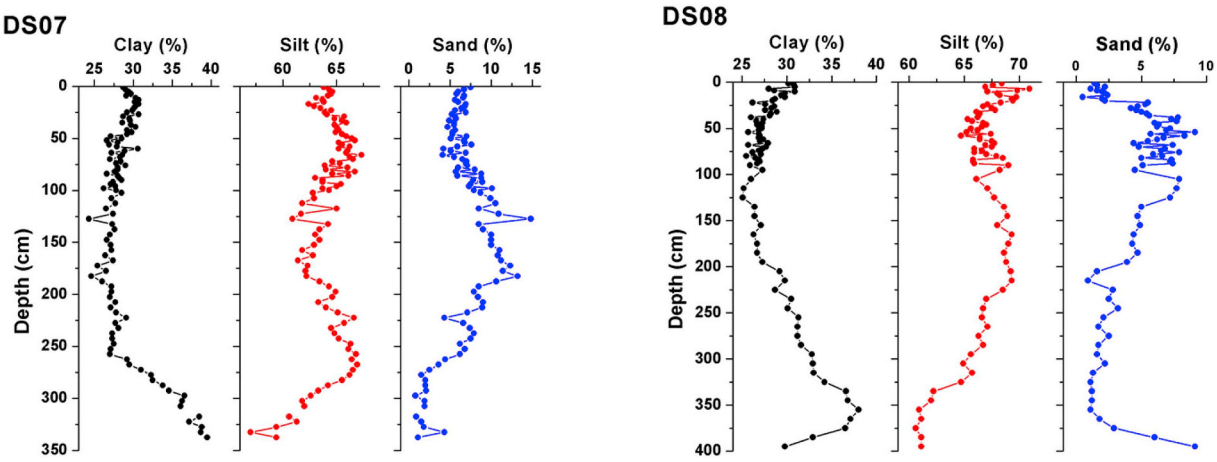

Fig. 2. Vertical profiles of grain size compositions for DS07 and DS08.

3.2. Iron speciation as indicated by Mössbauer spectra

Mössbauer spectroscopy is a powerful tool used for studying iron speciation. This is because different iron species show different sets of absorption peaks (Hilton et al., 1986). The Mössbauer spectra of typical samples are shown in Fig. 4. The fitting curves of the two sediment cores were similar. All samples from different depths could be classified into two doublets. According to the Mössbauer parameters, the doublet (D1) with higher isomer shifts and quadruple splitting could be attributed to paramagnetic high-spin ferrous Fe (para-Fe^{2+}) (Medina et al., 2006; Zheng et al., 2010). The smaller isomer shifts and quadruple splitting of the doublet (D2) were likely indicative of ferric compounds (para-Fe^{3+}). The para-Fe^{3+} probably originated from amorphous hydrated Fe (III) oxides and/or clay minerals (Manning et al., 1980; Torrance et al., 1986; Lougear et al., 2000).

According to the fitting results of the Mössbauer spectra, the relative

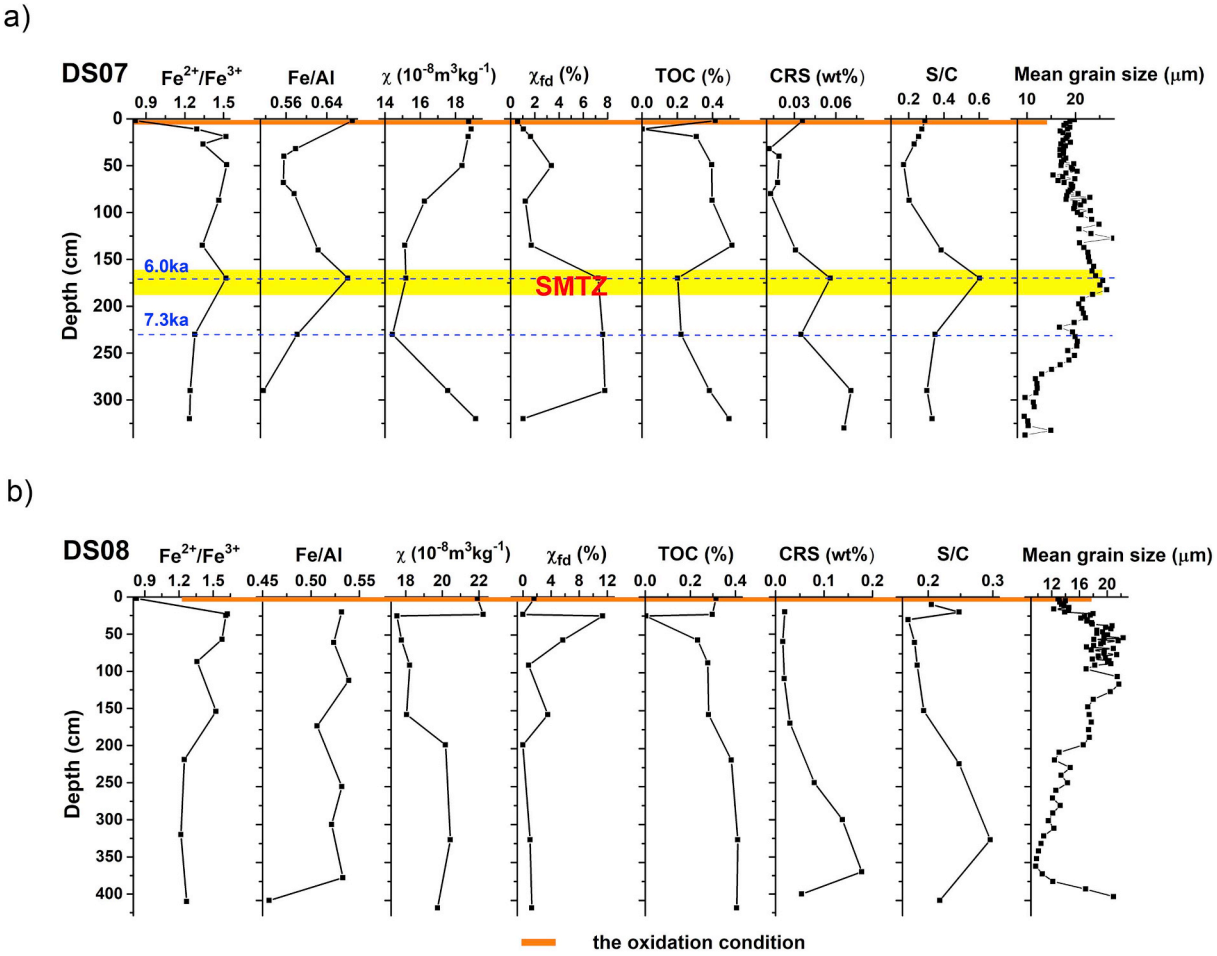

Fig. 3. Vertical profiles of Fe^{2+}/Fe^{3+}, Fe/Al, χ, χ_{fd}, TOC, CRS, the S/C ratio and mean grain size for the DS07 and DS08 sediment cores (data for Fe/Al, CRS, and S/C are from Hu et al. (2017)). The yellow zone indicates the SMTZ and the brown zone highlights oxidizing zone. (For interpretation of the references to color in this figure legend, the reader is referred to the Web version of this article.)

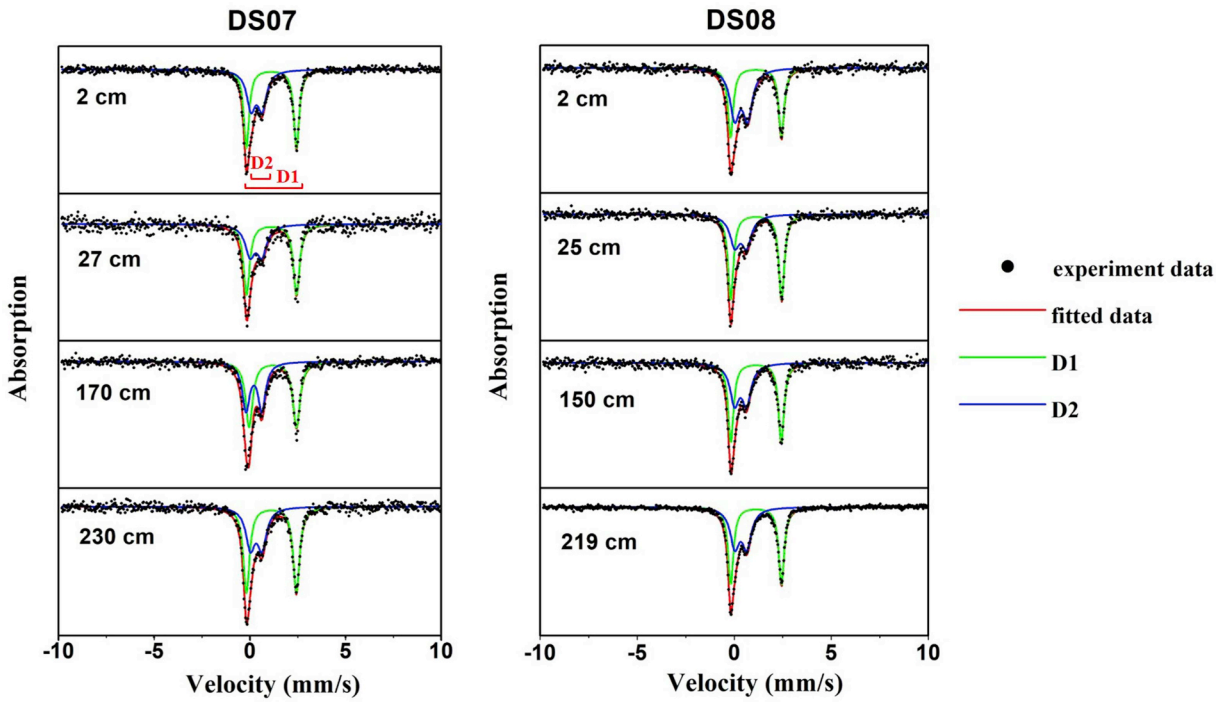

Fig. 4. Mössbauer spectra for the typical depths of DS07 and DS08.

Table 1
The fitting parameters in the Mössbauer spectra for DS07 and DS08.

Depth/cm	Iron species	Relative content%	IS/mm·s^{-1}	QS/mm·s^{-1}	Fe^{2+}/Fe^{3+}
DS07					
11.00	para- Fe^{2+}	56.40	1.127 ± 0.002	2.618 ± 0.004	1.29
	para- Fe^{3+}	43.60	0.348 ± 0.006	0.574 ± 0.009	
19.00	para- Fe^{2+}	60.30	1.189 ± 0.005	2.484 ± 0.010	1.52
	para- Fe^{3+}	39.70	0.192 ± 0.008	0.848 ± 0.016	
27.00	para- Fe^{2+}	57.30	1.126 ± 0.004	2.614 ± 0.009	1.34
	para- Fe^{3+}	42.70	0.352 ± 0.017	0.624 ± 0.026	
49.00	para- Fe^{2+}	60.40	1.131 ± 0.006	2.609 ± 0.011	1.52
	para- Fe^{3+}	39.60	0.315 ± 0.020	0.613 ± 0.030	
87.00	para- Fe^{2+}	59.40	1.117 ± 0.007	2.617 ± 0.014	1.46
	para- Fe^{3+}	40.60	0.345 ± 0.021	0.673 ± 0.035	
135.00	para- Fe^{2+}	57.20	1.121 ± 0.002	2.602 ± 0.004	1.34
	para- Fe^{3+}	42.80	0.350 ± 0.005	0.604 ± 0.008	
170.00	para- Fe^{2+}	60.30	1.125 ± 0.003	2.611 ± 0.005	1.52
	para- Fe^{3+}	39.70	0.329 ± 0.009	0.604 ± 0.013	
230.00	para- Fe^{2+}	56.10	1.198 ± 0.004	2.475 ± 0.007	1.28
	para- Fe^{3+}	43.90	0.208 ± 0.005	0.824 ± 0.009	
290.00	para- Fe^{2+}	55.40	1.127 ± 0.001	2.623 ± 0.003	1.24
	para- Fe^{3+}	44.60	0.328 ± 0.004	0.623 ± 0.006	
320.00	para- Fe^{2+}	55.30	1.126 ± 0.002	2.623 ± 0.004	1.24
	para- Fe^{3+}	44.70	0.344 ± 0.007	0.620 ± 0.011	
DS08					
23.00	para- Fe^{2+}	55.90	1.128 ± 0.003	2.640 ± 0.005	1.27
	para- Fe^{3+}	44.10	0.345 ± 0.010	0.570 ± 0.016	
25.00	para- Fe^{2+}	61.90	1.129 ± 0.002	2.624 ± 0.004	1.62
	para- Fe^{3+}	38.10	0.333 ± 0.009	0.608 ± 0.014	
57.00	para- Fe^{2+}	61.70	1.124 ± 0.003	2.631 ± 0.006	1.61
	para- Fe^{3+}	38.30	0.336 ± 0.010	0.618 ± 0.016	
87.00	para- Fe^{2+}	61.20	1.124 ± 0.002	2.616 ± 0.003	1.58
	para- Fe^{3+}	38.80	0.340 ± 0.007	0.601 ± 0.010	
154.00	para- Fe^{2+}	55.50	1.124 ± 0.003	2.602 ± 0.005	1.25
	para- Fe^{3+}	44.50	0.325 ± 0.008	0.617 ± 0.012	
219.00	para- Fe^{2+}	54.90	1.126 ± 0.001	2.618 ± 0.002	1.22
	para- Fe^{3+}	45.10	0.338 ± 0.003	0.618 ± 0.005	
320.00	para- Fe^{2+}	57.60	1.126 ± 0.001	2.610 ± 0.003	1.36
	para- Fe^{3+}	42.40	0.335 ± 0.006	0.552 ± 0.009	
410.00	para- Fe^{2+}	60.40	1.126 ± 0.002	2.618 ± 0.003	1.53
	para- Fe^{3+}	39.60	0.340 ± 0.006	0.612 ± 0.009	

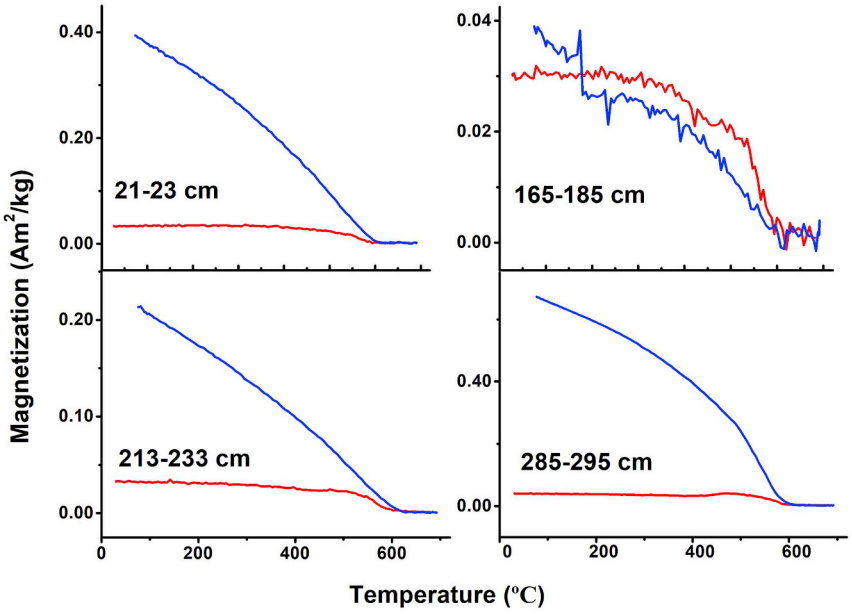

Fig. 5. Thermomagnetic curves of the typical DS07 samples. The red and blue lines indicate the heating and cooling processes, respectively. (For interpretation of the references to color in this figure legend, the reader is referred to the Web version of this article.)

contents of Fe^{2+} in DS07 and DS08 ranged from 45% to 60% (Table 1). The Fe^{2+}/Fe^{3+} ratios at these two sites, except for the upper layer (0–10 cm), were 1.22–1.62 and 1.23–1.52 (Fig. 3), respectively, indicating an overall reducing environment (Zheng et al., 2001; Zheng et al., 2001; Kuno et al., 2002). In DS07, the ratio fluctuated greatly, indicating oscillating redox conditions with depth. In DS08, the Fe^{2+}/Fe^{3+} ratio above 220 cm was greater than that below 220 cm (Fig. 3).

3.3. Magnetic susceptibility

χ values could typically reflect the concentration of ferrimagnetic minerals (e.g., magnetite) in the sediment (Thompson and Oldfield, 1986; Bloemendal et al., 1988; 1992). Moreover, χ_{fd} could be used to evaluate the contribution of very fine-grained magnetic grains to magnetic susceptibility (Rubio et al., 2001; Deng et al., 2004). The χ varied from 14 to 19 $\times 10^{-8}$ m^3kg^{-1} along the DS07 sediment core, with χ_{fd}% values ranging between 1 and 15% (Fig. 3). Meanwhile, the χ in DS08 ranged from 17 to 22 $\times 10^{-8}$ $m^3\,kg^{-1}$, and the χ_{fd}% values varied between 1 and 11% (Fig. 3).

To determine whether iron-bearing minerals changed with depth due to different diagenetic conditions, thermomagnetic analyses were performed on samples at representative depths (21–23 cm, 165–185 cm, 213–233 cm and 285–295 cm) in DS07 (Fig. 5). Fig. 5 shows that the variations in magnetization were similar at 21–23 cm, 213–233 cm and 285–295 cm during the heating and cooling processes, however, the sample curves of 165-185 cm depth were substantially different. Except for the 165-185 cm depth, the heating curves were characterized by a flat curve up to 500 °C, with a Curie point at 580 °C. This trend indicated that magnetite was the major magnetic carrier (Karlin and Levi, 1983; Thompson and Oldfield, 1986). The signals of magnetization during the cooling processes were higher than those during the heating processes at these three depths, implying that iron in paramagnetic minerals was transformed to magnetite when the samples were cooled (Horng and Chen, 2006; Liu et al., 2010). In contrast, the thermomagnetic curves at 165–185 cm were almost reversible, indicating minor transformation of paramagnetic minerals to magnetite during the heating and cooling processes (Fig. 5; Thompson and Oldfield, 1986; Kruiver et al., 2001; Liu et al., 2007a,b). All measured samples showed minor magnetization changes between 600 °C and 700 °C, indicating minor hematite in these samples (Thompson and Oldfield, 1986; Deng et al., 2001). Moreover, pyrite was not abundant in these sediment cores as indicated by the nearly unchanged magnetization signals during the heating processes (Thompson and Oldfield, 1986; Deng et al., 2001).

4. Discussion

4.1. Interpretation of the historical diagenetic environment via Fe speciation

From the relatively constant ratios of Ti/Al and Zr/Rb, Hu et al. (2017) assumed a relatively stable terrigenous input to the Dongsha area. Hence, based on the Fe^{2+}/Fe^{3+} ratios determined by Mössbauer spectroscopy, we could evaluate the relative paleo-depositional redox conditions at the DS07 and DS08 sites (Liu et al., 2007a,b; Zheng et al., 2010; Scholz et al., 2014). The results from the correlation analysis show that there is no significant relationship between χ and the mean grain size along the DS07 and DS08 sediment cores. Therefore, we assume that grain size did not cause the change in χ in the sediments at these two sites. Similar phenomena have also been observed in other sediment cores (Hu et al., 2012). Based on the assumption of relatively stable sources, magnetic characteristics were therefore assumed to be caused by early diagenesis in the DS07 and DS08 sites (Zhang et al., 2007; Hu et al., 2012).

In the upper intervals (0–10 cm) of DS07 and DS08, the Fe^{2+}/Fe^{3+} ratios were less than 1 (Fig. 3), indicating an oxidizing environment in the top layer of the sediment cores. However, the Fe^{2+}/Fe^{3+} ratios increased with depth due to increased reducing conditions (Martens and Berner, 1974; Boetius et al., 2000; Alagarsamy, 2006; Reeburgh, 2007; Sato et al., 2012).

The DS07 sedimentary profile was characterized by changing redox condition with depth. The Fe^{2+}/Fe^{3+} ratio had a maximum value around the 170 cm depth (Fig. 2), indicating that this depth was within highly reducing conditions as compared to adjacent layers (Zheng et al., 2001; Li et al., 2003). The corresponding χ showed a marked localized minimum, in which the χ_{fd} was higher, indicating the dissolution of magnetic minerals at this depth (Fig. 3). The TOC contents were relatively low at 150–200 cm, likely the result of organic matter mineralization (Thornton and McManus, 1994). In addition, Fig. 3 shows that there was a peak of Fe/Al in the 150 to 200 cm range. To minimize the influence of grain size on element enrichment in the environment,

element to Al ratios are used for normalization purposes (Helz et al., 1996; Zheng et al., 2010; Sato et al., 2012). As a result, the Fe/Al peak indicated a weak enrichment of authigenic iron-bearing minerals at this depth (Fig. 3). The CRS and S/C ratios at approximately 170 cm depth were the highest along the sediment column (Fig. 3; Hu et al., 2017). In the TOC-poor and methane-rich sediments, the AOM likely contributed to a significant fraction of sulfides, resulting in the substantial increases in the CRS and S/C ratios in the sediments at this depth (Sato et al., 2012). Therefore, it was assumed that methane seepage activity occurred at approximately the 170 cm depth causing a dissolution of magnetite via AOM (Bloemendal et al., 1988; Rowan et al., 2009), which was in agreement with the pore water results in which the AOM led to the consumption of sulfate at this depth in DS07 sediment core (Hu et al., 2015). Relative to the 170 cm , there were weaker reducing conditions in sediments below 230 cm depth. It was in good agreement with the lower Fe^{2+}/Fe^{3+} and S/C ratios, as well as the higher χ values. The mean grain size decreased in this zone, which may favor of the preservation of organic matter at these depths (Z. Liu et al., 2010, 2016).

For DS08, anaerobic conditions were also noted (Fig. 3). The Fe^{2+}/Fe^{3+} ratio, grain size, average χ and χ_{fd} above 220 cm were relatively high (Figs. 2 and 3). S/C and CRS reached maximum values at the 320–350 cm, but the Fe^{2+}/Fe^{3+}, Fe/Al and magnetic parameters were almost unchanged below the 220 cm depth (Hu et al., 2017). Hence, there was no obvious SMTZ in DS08. The mean grain size resultsof core DS08 revealed that the sedimentation might have been impacted by turbidites due to the substantial changes in grain sizes at approximately 350 cm depth, and the feature of maximum grain size and median grain size matching with the Passega C = M diagram (Fig. 3; Passega, 1964; Zheng et al., 2002; Hu et al., 2017). Thus, the AOM signals were inconsistent in DS08 (Hu et al., 2015, 2017). In addition, these uncorroborated trends may be due to the SMTZ in DS08 was deeper than the core length. In the case, these signals may not have been recorded in this sediment profile (Hu et al., 2017). The TOC and the clay contents trends were consistent but opposite to that of mean grain size, indicating that an absorption of organic matter in clay minerals could be responsible for the preservation of the organic matter with with increasing depth (Thornton and McManus, 1994; Chen et al., 2004). Additionally, the maximum values of S/C in DS08 were approximately 0.36, which was close to the average of S/C inoxic-suboxic marine sediments (~0.36; Berner, 1985; Hu et al., 2017). As demonstrated in previous study on methane seepage areas, paleo-redox indicators such as S/C were not able to provide information on bottom water chemistry during sedimentation but reflect the pore-water chemistry during the post-depositional stage (Berner, 1985; Sato et al., 2012).

4.2. Iron speciation as a proxy for AOM at seep sites

Near the SMTZ along cold seep sediments, AOM result in the dissolution of magnetite and the enrichment of iron sulfides, which cause low TOC and χ but high CRS, S/C and Fe^{2+}/Fe^{3+} ratios; therefore, these abnormalities are often used to indicate the existence of the SMTZ in sediments (Torrance et al., 1986; Lim et al., 2011; Sato et al., 2012; Suess, 2014). Similar phenomena were noted along the DS07 sediment column. Therefore, based on the results in this work, we assumed that there was methane seepage at approximately 170 cm in DS07 study site.

To better understand the conversion of iron-bearing mineral assemblages in the sedimentary environments of DS07, thermomagnetic analysis was used to distinguish different types of magnetic minerals in the SMTZ. Generally, when methane seepage occurs, ferrimagnetic iron oxides are often largely reduced. Subsequently, when ferrous iron reacts with sulfide, paramagnetic iron sulfides form and result in a substantial change in the magnetic signal (Karlin and Levi, 1983, 1985). However, this analysis failed to detect authigenic iron minerals, such as pyrite, at approximately 170 cm. The reason was probably that cold hydrocarbon-rich fluid seepage was active for a short period of time (approximately 1 ka; Hu et al., 2017). The dissolved Mo was more reactive with HS^- in pore water, which caused Fe to react with the less abundant HS^-; therefore, the iron sulfides contents were likely too low to be determined by thermomagnetic analysis, however, other iron-forms might occur (Canfield et al., 1992; Zheng et al., 2000; Formolo and Lyons, 2013; Hu et al., 2017). Here we show that combination of the Mössbauer spectroscopy with the magnetic susceptibility analysis was helpful for determining the Fe speciation, and allowed us to trace the methane seepage environment and understand the AOM-related processes (Roberts and Turner, 1993; Neretin et al., 2004). In the present work, the surface layers of the DS07 sediment was found to be oxic, and organic matter deposition was mainly coupled with oxygen and Fe reduction. However, in the paleo-SMTZ (150–200 cm), Fe hydroxides and ferrimagnetic magnetite could largely act as electron acceptors to oxidize the methane, resulting in the formation of paramagnetic, authigenic, iron-bearing minerals.

Compared with the pore water analysis, sediments could provide information about the environment during early diagenesis and reveal changes based on geochemical reactions through iron species and iron-bearing minerals. Hence, this study shows that iron species and magnetic minerals could offer information about methane seepage and changes in historical redox conditions.

5. Conclusions

Iron speciation is an effective proxy to trace the paleo-environment setting during early diagenesis and may be used to identify AOM-related processes such as when methane seepage occurred. In the present study, we found that there were overall anoxic (ferruginous) conditions in DS07 and DS08, indicated by the Fe^{2+}/Fe^{3+} ratios and their relative contents from Mössbauer spectra. For DS07, transient methane seepage activities occurred at approximately 170 cm. In the paleo-SMTZ (150-200 cm), ferrimagnetic magnetite was largely consumed during AOM process, however, the authigenic magnetic minerals were too low to be detected due to the apparent short methane seepage timeframe. For DS08 site, no obvious methane seepage activity was observed likely because the sedimentation may have been impacted by turbidites. In summary, the iron speciation and the magnetic mineralogy characterization, such as high Fe^{2+}/Fe^{3+}, Fe/Al, CRS and S/C, low χ and TOC, was successfully carried out at the SMTZ. The results suggested that iron speciation, combined with the magnetic mineralogy used here, is a promising tool to trace the redox conditions during early diagenesis and evaluate methane seepage in seep environments.

Acknowledgments

We thank the crew on the exploration ship of the Guangzhou Marine Geological Survey in September 2013 for helping us meet our scientific objectives. We are grateful to the colleagues who performed the sample collections during this cruise. We appreciate Dr. Lin for the geochemical analyses (Shanghai Institute of Applied Physics, CAS). Moreover, many thanks to Professor Christian Sanders for language revisions of the manuscripts. The study was partially supported by the National Natural Science Foundation of China (Grant No. 91228201) and the National Basic Research Program of China (973 Program) (Grant No. 2014CB441502).

Appendix A. Supplementary data

Supplementary data related to this article can be found at https://doi.org/10.1016/j.ecss.2019.04.015.

References

Alagarsamy, R., 2006. Distribution and seasonal variation of trace metals in surface sediments of the Mandovi estuary, west coast of India. Estuar. Coast Shelf Sci. 67,

333–339.
Berner, R.A., 1970. Sedimentary pyrite formation. Am. J. Sci. 268, 1–23.
Berner, R.A., 1985. Sulphate reduction, organic matter decomposition and pyrite formation. Phil. Trans. Roy. Soc. Lond. 315 (1531), 25–38.
Bloemendal, J., King, J.W., Hall, F.R., Doh, S.J., 1992. Rock magnetism of Late Neogene and Pleistocene deep-sea sediments: relationship to sediment source, diagenetic processes, and sediment lithology. J. Geophys. Res. 97 (B4), 4361–4375.
Bloemendal, J., Lamb, B., King, J., 1988. Paleoenvironmental implications of rock-magnetic properties of late Quaternary sediment cores from the eastern Equatorial Atlantic. Paleoceanography 3, 61–87.
Boetius, A., Ravenschlag, K., Schubert, C.J., Rickert, D., Widdel, F., Gieseke, A., Pfannkuche, O., 2000. A marine microbial consortium apparently mediating anaerobic oxidation of methane. Nature 407, 623–626.
Boetius, A., Wenzhöfer, F., 2013. Seafloor oxygen consumption fueled by methane from cold seeps. Nat. Geosci. 6, 725–734.
Borowski, W.S., Paull, C.K., Ussler III, W., 1996. Marine pore-water sulfate profiles indicate in situ methane flux from underlying gas hydrate. Geology 24, 655–658.
Campbell, K.A., 2006. Hydrocarbon seep and hydrothermal vent paleoenvironments and paleontology: past developments and future research directions. Palaeogeogr. Palaeoclimatol. Palaeoecol. 232 (2–4), 362–407.
Canfield, D.E., Raiswell, R., Bottrell, S.H., 1992. The reactivity of sedimentary iron minerals toward sulfide. Am. J. Sci. 292, 659–683.
Chen, Z., Saito, Y., Kanai, Y., Wei, T., Li, L., Yao, H., Wang, Z., 2004. Low concentration of heavy metals in the Yangtze estuarine sediments, China: a diluting setting. Estuar. Coast Shelf Sci. 60, 91–100.
Coey, J.M.D., 1975. Iron in a post-glacial lake sediment core; a Mössbauer effect study. Geochem. Cosmochim. Acta 39, 401–415.
Deng, C.L., Zhu, R.X., Jackson, M.J., Verosub, K.L., Singer, M.J., 2001. Variability of the temperature-dependent susceptibility of the Holocene eolian deposits in the Chinese loess plateau: a pedogenesis indicator. Phys. Chem. Earth, Part A 26, 873–878.
Deng, C., Zhu, R., Verosub, K.L., Singer, M.J., Vidic, N.J., 2004. Mineral magnetic properties of loess/paleosol couplets of the central loess plateau of China over the last 1.2 Myr. J. Geophys. Res. 109, B01103. https://doi.org/10.1029/2003JB002532.
Dewangan, P., Basavaiah, N., Badesab, F.K., Usapkar, A., Mazumdar, A., Joshi, R., Ramprasad, T., 2013. Diagenesis of magnetic minerals in a gas hydrate/cold seep environment off the Krishna–Godavari basin, Bay of Bengal. Mar. Geol. 340, 57–70.
Ellwood, B.B., Balsam, W.L., Roberts, H.H., 2006. Gulf of Mexico sediment sources and sediment transport trends from magnetic susceptibility measurements of surface samples. Mar. Geol. 230, 237–248.
Formolo, M.J., Lyons, T.W., 2013. Sulfur biogeochemistry of cold seeps in the Green Canyon region of the Gulf of Mexico. Geochem. Cosmochim. Acta 119, 264–285.
Helz, G.R., Miller, C.V., Charnock, J.M., Mosselmans, J.F.W., Pattrick, R.A.D., Garner, C.D., et al., 1996. Mechanism of molybdenum removal from the sea and its concentration in black shales: EXAFS evidence. Geochem. Cosmochim. Acta 60, 3631–3642.
Hilton, J., Long, G.J., Chapman, J.S., Lishman, J.P., 1986. Iron mineralogy in sediments. A Mössbauer study. Geochem. Cosmochim. Acta 50, 2147–2151.
Horng, C., Chen, K., 2006. Complicated magnetic mineral assemblages in marine sediments offshore of southwestern Taiwan: possible influence of methane flux on the early diagenetic process. Terr. Atmos. Ocean Sci. 17, 1009.
Hu, Y., Chen, L., Feng, D., Liang, Q., Xia, Z., Chen, D., 2017. Geochemical record of methane seepage in authigenic carbonates and surrounding host sediments: a case study from the South China Sea. J. Asian Earth Sci. 138, 51–61.
Hu, Y., Feng, D., Chen, L., Zheng, G., Peckmann, J., Chen, D., 2015. Using iron speciation in authigenic carbonates from hydrocarbon seeps to trace variable redox conditions. Mar. Petrol. Geol. 67, 111–119.
Hu, Y., Feng, D., Peckmann, J., Roberts, H.H., Chen, D., 2014. New insights into cerium anomalies and mechanisms of trace metal enrichment in authigenic carbonate from hydrocarbon seeps. Chem. Geol. 381, 55–66.
Hu, Z., Zhang, W., Dong, C., 2012. Influence of early diagenesis on magnetic properties of inner shelf deposits of the East China Sea. Quat. Sci. 32, 670–678 (in Chinese).
Karlin, R., Levi, S., 1983. Diagenesis of magnetic minerals in recent haemipelagic sediments. Nature 303, 327–330.
Karlin, R., Levi, S., 1985. Geochemical and sedimentological control of the magnetic properties of hemipelagic sediments. J. Geophys. Res. 90, 0373–10392.
Kasten, S., Freudenthal, T., Gingele, F.X., Schulz, H.D., 1998. Simultaneous formation of iron-rich layers at different redox boundaries in sediments of the Amazon deep-sea fan. Geochem. Cosmochim. Acta 62, 2253–2264.
Kuno, A., Zheng, G.D., Matsuo, M., Takano, B., Shi, J.A., Wang, Q., 2002. Mössbauer spectroscopic study on vertical distribution of iron species in sediments from Qinghai Lake, China. Hyperfine Interact. 141, 321–326.
Kruiver, P.P., Dekkers, M.J., Heslop, D., 2001. Quantification of magnetic coercivity components by the analysis of acquisition curves of isothermal remanent magnetization. Earth Planet. Sci. Lett. 189, 269–276.
Li, X., Lü, X., Sun, Y., 2003. Relation of active iron and redox environments in the sediments of Bohai Sea. Mar. Environ. Sci. 22, 20–24.
Li, L., Lei, X., Zhang, X., Sha, Z., 2013. Gas hydrate and associated free gas in the Dongsha Area of northern South China Sea. Mar. Petrol. Geol. 39, 92–101.
Lim, Y.C., Lin, S., Yang, T.F., Chen, Y.G., Liu, C.S., 2011. Variations of methane induced pyrite formation in the accretionary wedge sediments offshore southwestern Taiwan. Mar. Pet. Geol. 28, 1829–1837.
Liu, J., Zhu, R., Li, T., Li, A., Li, J., 2007a. Sediment－ magnetic signature of the mid-Holocene paleoenvironmental change in the central Okinawa Trough. Mar. Geol. 239, 19–31.
Liu, J., Chen, Z., Chen, M., Yan, W., Xiang, R., Tang, X., 2010. Magnetic susceptibility variations and provenance of surface sediments in the South China Sea. Sediment. Geol. 230, 77–85.
Liu, J., Qin, H., Kong, X., 2007b. Comparative researches on the magnetic properties of muddy sediments from the yellow sea and east China sea shelves and the korea strait. Quat. Sci. 27, 1031–1039 (in Chinese).
Liu, Z., Colin, C., Li, X., Zhao, Y., Tuo, S., Chen, Z., Huang, K.F., 2010. Clay mineral distribution in surface sediments of the northeastern South China Sea and surrounding fluvial drainage basins: source and transport. Mar. Geol. 277, 48–60.
Liu, Z., Zhao, Y., Colin, C., Stattegger, K., Wiesner, M.G., Huh, C.A., Huang, C.Y., 2016. Source-to-sink transport processes of fluvial sediments in the South China Sea. Earth Sci. Rev. 153, 238–273.
Lougear, A., Grodzicki, M., Bertoldi, C., Trautwein, A.X., Steiner, K., Amthauer, G., 2000. Mössbauer and molecular orbital study of chlorites. Phys. Chem. Miner. 27, 258–269.
Lyons, T.W., Severmann, S., 2006. A critical look at iron paleoredox proxies: new insights from modern euxinic marine basins. Geochem. Cosmochim. Acta 70, 5698–5722.
Manning, P.G., Jones, W., Birchall, T., 1980. Mössbauer spectral studies of iron-enriched sediments from Hamilton Harbor, Ontario. Can. Mineral. 18, 291–299.
Martens, C.S., Berner, R.A., 1974. Methane production in the interstitial waters of sulfate-depleted marine sediments. Science 185, 1167–1169.
Medina, G., Tabares, J.A., Alcázar, G.A.P., Barraza, J.M., 2006. A methodology to evaluate coal ash content using siderite Mössbauer spectral area. Fuel 85, 871–873.
Neretin, L.N., Böttcher, M.E., Jørgensen, B.B., Volkov, I.I., Lüschen, H., Hilgenfeldt, K., 2004. Pyritization processes and greigite formation in the advancing sulfidization front in the upper Pleistocene sediments of the Black Sea 1. Geochem. Cosmochim. Acta 68, 2081–2093.
Novosel, I., Spence, G.D., Hyndman, R.D., 2005. Reduced magnetization produced by increased methane flux at a gas hydrate vent. Mar. Geol. 216, 265–274.
Passega, R., 1964. Grain size representation by CM patterns as a geologic tool. J. Sediment. Petrol. 34, 830–847.
Passier, H.F., Dekkers, M.J., Lange, G.J.D., 1998. Sediment chemistry and magnetic properties in an anomalously reducing core from the eastern Mediterranean Sea. Chem. Geol. 152, 287–306.
Pyzik, A.J., Sommer, S.E., 1981. Sedimentary iron monosulfides: kinetics and mechanism of formation. Geochem. Cosmochim. Acta 45, 687–698.
Reeburgh, W.S., 2007. Oceanic methane biogeochemistry. Chem. Rev. 107, 486–513.
Riedinger, N., Pfeifer, K., Kasten, S., Garming, J.F.L., Vogt, C., Hensen, C., 2005. Diagenetic alteration of magnetic signals by anaerobic oxidation of methane related to a change in sedimentation rate. Geochem. Cosmochim. Acta 69, 4117–4126.
Roberts, A.P., Turner, G.M., 1993. Diagenetic formation of ferrimagnetic iron sulphide minerals in rapidly deposited marine sediments, South Island, New Zealand. Earth Planet. Sci. Lett. 115, 257–273.
Rowan, C.J., Roberts, A.P., Broadbent, T., 2009. Reductive diagenesis, magnetite dissolution, greigite growth and paleomagnetic smoothing in marine sediments: a new view. Earth Planet. Sci. Lett. 277, 223–235.
Rubio, B., Pye, K., Rae, J.E., Rey, D., 2001. Sedimentological characteristics, heavy metal distribution and magnetic properties in subtidal sediments, Ria de Pontevedra, NW Spain. Sedimentology 48, 1277–1296.
Sato, H., Hayashi, K.I., Ogawa, Y., Kawamura, K., 2012. Geochemistry of deep sea sediments at cold seep sites in the Nankai Trough: insights into the effect of anaerobic oxidation of methane. Mar. Geol. 323, 47–55.
Scholz, F., McManus, J., Mix, A.C., Hensen, C., Schneider, R.R., 2014. The impact of ocean deoxygenation on iron release from continental margin sediments. Nat. Geosci. 7, 433.
Suess, E., 2014. Marine cold seeps and their manifestations: geological control, biogeochemical criteria and environmental conditions. Int. J. Earth Sci. 103, 1889–1916.
Thompson, R., Oldfield, F., 1986. Environmental Magnetism. Allen and Unwin, Winchester Mass, pp. 227.
Thornton, S.F., McManus, J., 1994. Application of organic carbon and nitrogen stable isotope and C/N ratios as source indicators of organic matter provenance in estuarine systems: evidence from the Tay Estuary. Scotland. Estuar. Coast. Shelf Sci. 38, 219–233.
Torrance, J.K., Hedges, S.W., Bowen, L.H., 1986. Mössbauer spectroscopic study of the iron mineralogy of post-glacial marine clays. Clay Clay Miner. 34, 314–322.
Vandenberghe, R.E., De Grave, E., De Bakker, P.M.A., 1994. On the methodology of the analysis of Mössbauer spectra. Hyperfine Interact. 83, 29–49.
Yan, P., Deng, H., Liu, H., 2006. The geological structure and prospect of gas hydrate over the Dongsha Slope, South China Sea. Terr. Atmos. Ocean Sci. 17, 645.
Zachara, J.M., Kukkadapu, R.K., Gassman, P.L., Dohnalkova, A., Fredrickson, J.K., Anderson, T., 2004. Biogeochemical transformation of Fe minerals in a petroleum-contaminated aquifer. Geochem. Cosmochim. Acta 68, 1791–1805.
Zhang, W., Dai, X., Zhang, F., Shi, Y., Yu, L., J A, D., 2007. Magnetic properties of sediments from the Chaohu lake for the last 7000 years and their implications for the evolution of Asian monsoon. Quat. Sci. 27, 1053–1062 (in Chinese).
Zheng, G., Takano, B., Kuno, A., Matsuo, M., 2001. Iron speciation in modern sediment from Erhai Lake, southwestern China Redox conditions in an ancient environment. Appl. Geochem. 16, 1201–1213.
Zheng, G., Lang, Y., Takano, B., Matsuo, M., Kuno, A., Tsushima, H., 2002. Iron speciation of sliding mud in Toyama Prefecture, Japan. J. Asian Earth Sci. 20, 955–963.
Zheng, G., Fu, B., Takahashi, Y., Kuno, A., Matsuo, M., Zhang, J., 2010. Chemical speciation of redox sensitive elements during hydrocarbon leaching in the Junggar Basin, Northwest China. J. Asian Earth Sci. 39, 713–723.
Zheng, Y., Anderson, R.F., Van Geen, A., Kuwabara, J., 2000. Authigenic molybdenum formation in marine sediments: a link to pore water sulfide in the Santa Barbara Basin. Geochem. Cosmochim. Acta 64, 4165–4178.